EFFECTIVE SOURCE TERM DISCRETIZATIONS FOR HIGHER ACCURACY FINITE VOLUME DISCRETIZATION OF PARABOLIC EQUATIONS

YAW KYEI
DEPARTMENT OF DECISION SCIENCES, NORTH CAROLINA CENTRAL UNIVERSITY, DURHAM, NC 27707,

Abstract

A finite volume method is applied to develop space-time discretizations for parabolic equations based on an equation error method. A space-time expansion of the local equation error based on flux integral formulation of the equation is first designed using a desired framework of neighboring quadrature points for the solution and local source terms. The quadrature weights are then determined through a minimization process for the error which constitutes all local compact fluxes about each centroid within the computational domain. In utilizing a local source term distribution to account for diffusive fluxes, the right minimizing weights and collocation points including sub-grid points for the source terms may be determined and optimized for higher accuracies as well as robust higher-order computational convergence. The resulting local residuals form a more complete description of the truncation errors which are then utilized to assess the computational performances of the resulting schemes. The effectiveness of the method is demonstrated by the results and analysis of the schemes.

Key words. Finite volume method, space-time control volume, local equation error expansion, higher-order convergence, Heat equation, one-step scheme, numerical domain of dependence, general weighted quadrature, conservative flux integral

1. Introduction

To achieve robust higher computational accuracies for the heat equation, the discretization method must be efficient in characterizing the fundamental local fluxes of the diffusion within the space-time computational domain in order to conserve small and large scale attributes as much as possible. This requires that the associated discretization error for the equation must be comprehensively formulated to allow for local fluxes to as many neighboring grid points as possible to mimic flow in the continuous system. In this article we present a space-time finite volume differencing framework for constructing one- and two-step higher-order finite volume schemes for the heat equation based on the distribution of local radial fluxes about their centroid. After rewriting the equation into a conservative flux integral form over the space-time cylindrical domain, it is reformulated into a general quadrature approximation form of undetermined coefficients. This is accomplished by utilizing general weighted quadratures to approximate

the flux integral operators using a unified space-time solution expansion in a comprehensive approach that preserves operator properties of the equation about each grid point interior to the space-time domain.

By formulating the equation this way, the resulting numerical schemes describe a synchronized time evolution representation [13, 26] of the diffusion that allows for a more complete local compact flux characterization about each space-time grid point. This guarantees higher conservation of local fluxes in regulating transport and rendering the schemes more uniformly higher-order accurate compared with similar implementations of traditional finite difference schemes.

The finite volume differencing formulation is very systematic in a way that allows for flexible adaptive control volumes which are basically identified by their centroid grid point values and the adopted neighboring space-time points including sub-grid points. All such neighboring grid-point values in space and time may be utilized to set up the weighted quadrature approximation of the integral formulation for the equations and therefore nearby control volumes overlap [34].

As part of the motivation for this work, we seek to achieve consistent higher-order convergence rates by utilizing unified local space-time expansions for the solution and the source terms rather than simplifying the discretization on space-time control volumes as discretization in space followed by a discretization in time [26] as in traditional semi-discretization approaches. This ensures that the right space-time flow characteristics governed by the equation about the centroid of the desired neighboring points are accounted for which ensures uniform higher-order convergence rates. That is, traditional semi-discretization methods fail to produce local mesh refinements in the space-time domains and as such make it difficult for such schemes to accurately track local regularities of the solution without the need to take small time steps [9]. Therefore, a unified space-time formulation that combines space and time into a single differentiable manifold locally eliminates the need for small time steps in order to achieve consistent higher-order convergence rates and hence is computationally cost effective [4,16]. The approximation of the equation on the local space-time manifold allows for coordinating new time steps with weighted quadratures of grid points within the domains of dependence to mimic the natural evolution of the continuous system [8].

There are similar approaches of space-time methods using finite element theory for hyperbolic systems [9,15] where the finite elements for the numerical methods are constructed in time and space simultaneously. Our approach is similar to the space-time discontinuous Galerkin method [33] but uses uniform spatial resolutions on finite difference stencils and allows for new time steps to be determined separately based on local residual error expansions in order to achieve consistent higher-order convergence rates. Thus, grid points for the new time steps may be determined as a function of spatial resolution and local flux coefficients in order to regulate growth of local errors similar to the Arbitrary Lagrangian-Eulerian technique [2,7,25] where grid points may be moved in a prescribed manner. In a similar work [14], the quadrature points are adjusted slightly from conventional points in order to reduce dispersion error in finite element methods. Furthermore, our approach is also similar to the ADER approach that involves defining numerical fluxes and numerical sources [32]. We define the numerical fluxes and sources using weighted quadratures of the associated grid points. Thus the overall accuracy of the space-time discretization of the equation increases as the number of quadrature points within the domains of influence used in constructing the numerical fluxes and sources about each grid point increases. We determine the weights to annihilate the coefficients of the partial derivatives through the minimization

of a space-time error expansion for the equation. As such, there is no need to use a solution reconstruction method per grid point to approximate partial derivatives in the solution expansion as in the ADER approach and thus resulting schemes have relatively less implementation costs per grid point.

The paper is organized as follows: In Section 2, we present the general space-time finite volume differencing framework and the design for the schemes by describing the discretization of the parabolic equation in one spatial dimension where the space-time domain is two-dimensional. In Section 3, we provide further details on the weighted quadrature method and the constrained minimization of the space-time equation error expansion to determine the quadrature weights the desired schemes. In Section 4, we provide a generalized one-step three-point discretization of the parabolic equation as well as stability and accuracy analyses of the schemes. Local accuracy improvements through alternate parameterized schemes based on the equation error residuals are discussed. Subsequently, the source term collocations for a list of one-step schemes are discussed including strategies for utilizing source term distributions to improve solution accuracies. Numerical results demonstrating the effectiveness of the methods are illustrated in Section 5 where the source term collocations for improved local accuracies are compared with traditional methods. We briefly discuss extensions to higher spatial dimensions and present conclusions in Section 6.

2. Space-time finite volume differencing framework.

Consider the parabolic transport problem below of finding $u = u(x, t)$ such that

$$\begin{aligned} \frac{\partial u}{\partial t} &= \sigma \Delta u + q \quad \text{in } \Omega \times (0,T],\ x \in \Omega = [a,b] \\ u(x,0) &= u_0(x) \quad \text{for } x \in \Omega \\ u &= g(x,t) \quad \text{in} \quad \Gamma \times (0,T] \end{aligned} \tag{2.1}$$

where q and g are assumed to be sufficiently smooth. We use a space-time unified framework to construct stable, conservative, and higher-order accurate finite volume schemes for (2.1) in a comprehensive approach with accuracy improvements over semi-discretization approaches. The approximation of local fluxes [11] needed to ensure uniform higher-order convergence rates is improved by the unified space-time formulation. Thus, the equation (2.1) is reformulated over a space-time domain rather than discretizing in separate coordinate directions [30].

We thus rewrite (2.1) in an integral form over the space-time domain such that

$$\int_{\Omega_T} u_t \, dxdt = \int_{\Omega_T} (\sigma \Delta u + q)\, dxdt, \tag{2.2}$$

where Ω_T is the space-time domain which is the closure of $\Omega \times (0,T]$ in R^2. Using the divergence theorem, (2.2) is rewritten into a flux integral balance form as

$$\int_{\partial\Omega_T} u \cdot \eta_t \, dx = \int_{\partial\Omega_T} \sigma \nabla u \cdot \nu \, dS + \int_{\Omega_T} q \, dxdt \tag{2.3}$$

over the space-time cylinder Ω_T where v is the unit outward normal to the surface S of Ω_T which is a function of time and space, and η_t is the component in the temporal direction.

Now, consider the two-dimensional space-time domain Ω_T as partitioned into space-time control volumes where each control volume is centered on a space-time grid point with a regular distribution of neighboring space-time grid points. Thus, each grid point has a cloud of quadrature points that describes the control volume which overlaps [34] with the distribution of grid points for neighboring control volumes. The interlocking configurations created by these overlaps help to effectively capture more local fluxes to neighboring points across different time levels necessary for higher level of conservation and consistent higher-order accuracy. Other space-time methods [4,9,27,28] describe the local partitioning as finite space-time slabs where balance of fluxes is considered [28].

Following a similar characterization of the local space-time domain [28], consider a partition of the time interval $[0,T]$ by $0 = t_0 < t_1 < \cdots < t_N = T$ and the domain $[a, b] \in \mathrm{R}$ by $a = x_0 < x_1 < \cdots < x_M = b$ such that the space-time control volume is $\mathbf{Q}^n{}_m = [x_m - h, x_m + h] \times [t_n - 1, t_{n+1}]$ and illustrated in Figure 2.1. Each control volume $\mathbf{Q}^n{}_m$ consists of a centroid X_0 with a compact cloud of quadrature points $X_1, X_2, X_3, X_4, X_5, X_6, X_7,$ and X_8 for the solution as depicted in Figure 2.1 where $\mathbf{Q}^n{}_m$ overlaps with control volumes centered on all these surrounding grid points.

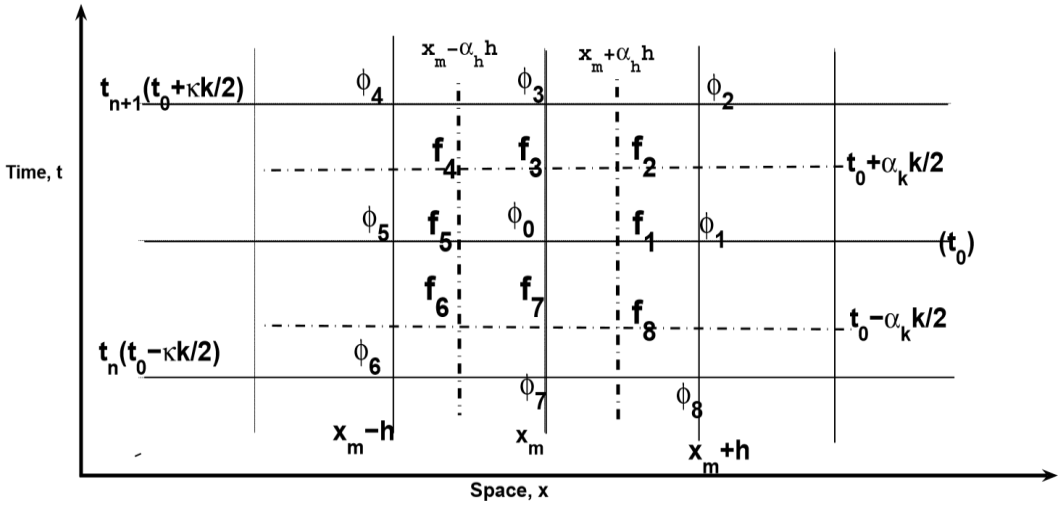

Fig. 2.1. *Control volume* $\mathbf{Q}^n{}_m$ *centered on* $X_0(t_0, x_m)$ *with local uniform compact cloud of quadrature grid functions* φ_i*s for the solution and* f_i*s for the local source terms. Given the spatial resolution h,* κ *is chosen to regulate the leading coefficients of the residual error. The collocation points* α_h *and* α_k *for the source term are also to be determined.*

We describe the flux integral balance equation (2.3) on each control volume $\mathbf{Q}^n{}_m$ by

$$\int_{\partial \mathbf{Q}^n_m} u \cdot \eta_{kh}\, dx = \int_{\partial \mathbf{Q}^n_m} \sigma \nabla u \cdot \nu_{kh}\, dS_{kh} + \int_{\mathbf{Q}^n_m} q\, dxdt \qquad (2.4)$$

where v_{kh} is the unit outward normal vector to S_{kh}, the space-time surface of $\mathbf{Q}^n{}_m$ and η_{kh} is the component in the temporal direction on $\mathbf{Q}^n{}_m$.

Now, the left hand side of (2.4) that describes the time rate of change of u within $\mathbf{Q}^n{}_m$ depends on local diffusive fluxes and source term distribution on the local two-dimensional space-time manifold about (x_m,t_n). We thus rewrite (2.4) to indicate the dependence of the change in u between the initial time frame $\Gamma_0(h,k)$ and the new time frame $\Gamma_f(h,k)$ on $\mathbf{Q}^n{}_m$ by

$$\int_{\Gamma_f(h,k)} u\,dx - \int_{\Gamma_0(h,k)} u\,dx = \int_{\partial \mathbf{Q}^n_m} \sigma \nabla u \cdot \nu_{kh}\,dS_{kh} + \int_{\mathbf{Q}^n_m} q\,dxdt \qquad (2.5)$$

where $\Gamma_0(h,k)$ and $\Gamma_f(h,k)$ are respectively determined by the times $t_n - k/2$ and $t_n + k/2$ and their associated spatial distributions of grid points.

On each control volume, local space-time fluxes are to be best captured by a weighted quadrature approximation of the flux integrals in (2.5) in order to rightly incorporate quadrature points within the domain of dependence on the initial time frame $\Gamma_0(h,k)$ subject to the distribution of grid points [31] and the space-time expansions adopted. We remark that the local flux integral balance set up in (2.4) is very similar to other work [6,10,22,23,28,30]. However, to capture the flux at a higher order accuracy we adopt a unified space-time expansion for u to formulate the fluxes in a multivariate sense and then utilize the differencing of the quadrature approximations of the integrals to capture local compact fluxes through the minimization of a local discretization error for (2.5). By formulating local fluxes comprehensively using all compact grid point function values for the solution and possibly sub-grid values for the source terms, control volumes of any shape (regular or irregular) in other formulations [10] work with this methodology.

To approximate (2.5) about each centroid, we adopt a unified [24] space-time Taylor's expansion φ to locally describe the local space-time manifold of u by

$$\phi(x_m + x, t_n + t) = \sum_{q=0}^{\infty} \sum_{i+j=q} \frac{C(q,i)}{q!} \frac{\partial^q \phi}{\partial x^i \partial t^j}(t_n, x_m) x^i t^j \qquad (2.6)$$

where φ is assumed to be smooth enough. We carry out the expansion about the half-time point to ensure uniform discretization and to more easily formulate fluxes (diagonal transient and diffusive fluxes) about (t_n, x_m) from all neighboring points subject to available degrees of freedom.

We then constrain the coefficients of the terms φ_{xt}, φ_{xxt}, φ_{xtt}, etc in (2.6) by higher-order spatial and temporal derivatives of the equation and introduce terms like f_{xt}, f_{xxt}, f_{xtt} to reflect more local regularities of the equation by way of the Cauchy-Kovalevskaya procedure [23].

To achieve the objective of obtaining a robust higher-order discretization for the equation (2.5) and to guarantee uniform convergence rates, the source term must be collocated effectively in order to efficiently capture the associated local variations in source term distribution. Hence, we use a local operator action on the solution expansion φ to define the source term as

$$f(x_m + x, t_n + t) = \triangle_\kappa \left\{ \sum_{q=0}^{\infty} \sum_{i+j=q} \frac{C(q,i)}{q!} \frac{\partial^q \phi}{\partial x^i \partial t^j}(t_n, x_m) x^i t^j \right\} \qquad (2.7)$$

where κ represents the action of the differential operator describing the unique local description of 2.1 such that

$$f_0 = f(x_m, t_n) = \triangle_\kappa \phi|_{(x_m,t_n)} := (\phi_t - \sigma\Delta\phi)|_{(x_m,t_n)}. \tag{2.8}$$

A unified space-time equation error expansion for the flux integral representation (2.5) is then formulated about each centroid by using general weighted quadrature approximations for the integral operators. By utilizing quadratures of the grid point values of the solution and the source term to approximate the equation between times $t_n + k/2$ and $t_n - k/2$, allows for adaptive use of grid points to ensure improvements in local accuracies. Thus, different geometries of grid functions on the control volume may be adapted to suit specific situations like near irregular boundaries [1,17]. Furthermore, local physical parameters of the equation are efficiently represented by the source term (2.7) in accounting for local fluxes in the balance formulation (2.5).

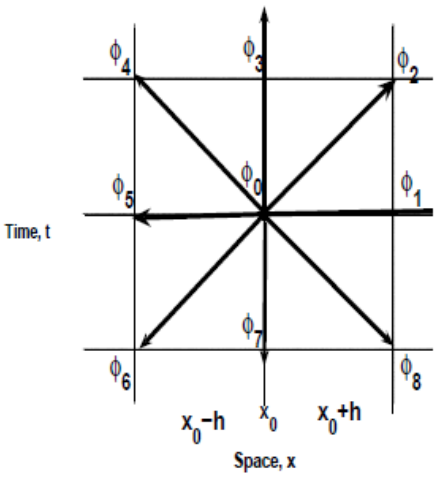

FIG. 2.2. *Space-time control volume with centroid at (x_m, t_n) indicating the geometry of eight local directional space-time fluxes about the centroid.*

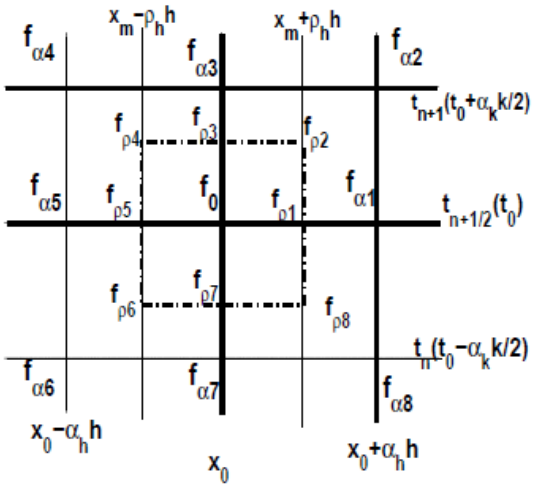

FIG. 2.3. *Space-time control volume with centroid at (x_m, t_n) indicating the geometry of fourteen local directional fluxes about the centroid.*

As illustrated by the distribution of the grid points about the centroid (x_m,t_n) in Figure 2.2, the local diffusive flux $\sigma\nabla\varphi$ has contributions (direct or indirect) from all the neighboring solution values on the local space-time manifold containing the solution. We therefore approximate $\sigma\nabla\varphi$ about (x_m,t_n) by the generalized quadrature rule

$$\int_{\partial \mathbf{Q}_m^n} \sigma\nabla\phi \cdot \nu_{kh}\, dS_{kh} \approx \sum_{i=1}^{n_i} w_i(\phi_i - \phi_0) \quad \text{such that} \quad w_0 = \sum_{i=1}^{n_i} w_i, \tag{2.9}$$

where n_i the number of neighboring cloud of points to be adopted, and w_i is the weight for the local directional flux $\varphi_i - \varphi_0$.

We now write the residual $R(u)$ of the flux integral formulation (2.5) on each two-dimensional space-time control volume $\mathbf{Q}^n{}_m$ as

$$R(u) = \int_{\partial \mathbf{Q}^n_{m\, t_{n+1}}} u\, dx - \int_{\partial \mathbf{Q}^n_{m\, t_{n-1}}} u\, dx - \int_{\partial \mathbf{Q}^n_m} \sigma \nabla u \cdot \nu_{kh}\, dS_{kh} - \int_{\mathbf{Q}^n_m} q\, dxdt. \tag{2.10}$$

Then a discrete minimax approach is sought to approximate (2.10) by minimizing a local equation error expansion formulated for $R(u)$ using generalized weighted quadrature approximations of the flux integrals. Thus, the local equation error expansion R_{kh} about each centroid grid point is described as the generalized quadrature approximations of the flux integrals on the space-time control volume by

$$R_{kh} = \sum_{\partial \mathbf{Q}^n_{m\, t_{n+1}}} \alpha_i \phi_i - \sum_{\partial \mathbf{Q}^n_{m\, t_{n-1}}} \beta_i \phi_i - \sum_{\partial \mathbf{Q}^n_m} w_i(\phi_i - \phi_0) - \sum_{\mathbf{Q}^n_m} v_i f_i \tag{2.11}$$

where the weights w_i, α_i, β_i, and v_i are to be determined by eliminating the leading coefficients of the error (2.11). In [14], a similar modified generalized integration rule is implemented where the quadrature weights are assumed to be units but the quadrature points are adjusted slightly from conventional points in order to reduce dispersion error in finite element methods.

Clearly, the framework for the local error expansion (2.11) allows for sub-grid collocations of the local source term to be utilized in the discretization. We therefore formulate the approximation of the more balanced flux integral form of the equation (2.11) about the centroid of the control volume $Q^n{}_m$ by

$$R_{kh} = \sum_{\partial \mathbf{Q}^n_{m\, t_{n+1}}} \alpha_i \phi_i - \sum_{\partial \mathbf{Q}^n_{m\, t_{n-1}}} \beta_i \phi_i - \sum_{\partial \mathbf{Q}^n_m} w_i(\phi_i - \phi_0) - \sum_{\mathbf{Q}^n_m} v_i f_i \tag{2.12}$$

where $\varphi_i = \varphi(x_0 + ih)$, $f_i = f(x_0 + \pi_i h)$. While the nodes for the solution φ_i are fixed, the nodes for the source term f_i are not fixed as in a generalized Gaussian quadrature approach but allowed to be symmetric about the centroid as schematically described in Figure 2.1. Thus, the weights

$\{\alpha_i, \beta_i, w_i, v_i\}$ and the corresponding nodes α_is are to be optimally determined through the minimization process of the local equation error expansion.

In this work, the nodes for the solutions φ_i are fixed but the nodes and weights for the source term f_i are to be determined to minimize and regulate residual error expansion R_{kh} which constitutes the dissipation and dispersion errors associated with the discretization. As additional points are introduced in the quadrature approximations, the level of local accuracy improves. However, given a fixed number and distribution of points on the control volume, we seek the optimal combination of weights and nodes to minimize the residual error expansion R_{kh} as much as possible and to stabilize the resulting schemes. Determining the weights to minimize the space-time error expansion ensures that the dynamic weights may be effectively constrained to render the resulting schemes local extremum diminishing (LED) [18]. The constraints in the minimization process include:

- For a non uniform grid, the task of determining the collocation parameters is tedious as reported in a similar work in [12]. However, the symmetric collocations of the grid points eliminates odd powers and reduces the complexity of the error [31].
- The weights of f_i and φ_i are constrained to ensure M-matrix property for the resulting system matrices [3] and to guarantee faster convergence for iterative methods in solving the resulting linear systems [3,24].

- Other constraints include restrictions on the weights in order to produce desired schemes as in one-step or two-step implicit or explicit schemes.

3. A Space-time finite volume discretization of parabolic equations in one spatial dimension

In this section, we provide additional details on the unified method of construction for the space-time discretizations. We recast the full space-time discretization of (2.5) as determining the future updates of u on the control volume tied with current and past distributions to describe the natural dynamics of the diffusion within the control volume. For the infinite dimensional settings on each control volume interior to $\Omega_T \in R^2$, the balance equation for the conserved quantity u is

$$\int_{\partial \mathbf{Q}^n_m t_{n+1}} u\,dx - \int_{\partial \mathbf{Q}^n_m t_n} u\,dx = \int_{\partial \mathbf{Q}^n_m} \sigma \nabla u\, dS_{kh} + \int_{\mathbf{Q}^n_m} q\,dxdt \qquad (3.1)$$

where $\partial \mathbf{Q}^n_m tn$ and $\partial \mathbf{Q}^n_m tn+1$ describe the initial and final time-boundaries of $\mathbf{Q}^n_m$, and S_{kh} is the total space-time boundary surface of $\mathbf{Q}^n_m$. The framework of this approach is similar to the finite volume element method [6] and the finite-dimensional approximation of (3.1) that describes the dynamics of the solution expansion φ about
(x_m, t_n) is given by the local quadrature formulation

$$\sum_{\partial \mathbf{Q}^n_m t_{n+1}} \alpha_i \phi_i^{n+1} - \sum_{\partial \mathbf{Q}^n_m t_n} \beta_i \phi_i^{n-1} = \sum_{\partial \mathbf{Q}^n_m} w_i \nabla \phi_i + \sum_{\mathbf{Q}^n_m} v_i f_i \qquad (3.2)$$

subject to

$$w_0 = \sum_{i=1}^{8} w_i, \quad \sum_{i=2}^{4} \alpha_i = \frac{1}{k}, \quad \sum_{i=6}^{8} \beta_i = \frac{1}{k}, \quad \sum_{i=0}^{n_f} v_i = 1. \qquad (3.3)$$

.

The grid functions for the solution φ_i are defined by

$$\begin{aligned}
&\phi_3 = \phi_i^{n+1} := \phi(x_m, t_n + \kappa k/2), && \phi_7 = \phi_i^n := \phi(x_m, t_n - \kappa k/2),\\
&\phi_2 = \phi_{i+h}^{n+1} := \phi(x_m + h, t_n + \kappa k/2), && \phi_4 = \phi_{i-h}^{n+1} := \phi(x_m - h, t_n + \kappa k/2),\\
&\phi_8 = \phi_{i+h}^{n} := \phi(x_m + h, t_n - \kappa k/2), && \phi_6 = \phi_{i-h}^{n} := \phi(x_m - h, t_n - \kappa k/2)
\end{aligned} \qquad (3.4)$$

where κ is to be determined from the residual of the local equation error expansion (2.11) and $\varphi_0 := \varphi(x_m, t_n)$ is the grid function value for the solution at the centroid of the control volume. The parameter, κ, a dimensionless time measure is the diffusive rate to changes in time where a large value indicates faster propagation through the control volumes [29]. The grid functions for the source terms f_i, also given by

$$
\begin{aligned}
f_3 = f_i^{n+1} &:= f(x_m, t_n + \alpha_k k/2), & f_7 = f_i^n &:= f(x_m, t_n - \alpha_k k/2),\\
f_2 = f_{i+h}^{n+1} &:= f(x_m + \alpha_h h, t_n + \alpha_k k/2), & f_4 = f_{i-h}^{n+1} &:= f(x_m - \alpha_h h, t_n + \alpha_k k/2),\\
f_8 = f_{i+h}^{n} &:= f(x_m + \alpha_h h, t_n - \alpha_k k/2), & f_6 = f_{i-h}^{n} &:= f(x_m - \alpha_h h, t_n - \alpha_k k/2),\\
f_1 = f_{i+h}^{n+1/2} &:= f(x_m + \alpha_h h, t_n), & f_5 = f_{i-h}^{n+1/2} &:= f(x_m - \alpha_h h, t_n) \qquad (3.5)
\end{aligned}
$$

where the nodes for f_i parameterized by α_k and α_h and their weights v_i are to be determined and $f_0 := \varphi(x_m,t_n)$ is the grid function value for the source term at the centroid. To ensure robust higher-order accuracies for the discretization, the time step k parameterized by κ is to be determined for a given resolution h through the minimization to regulate the growth of the residual errors in the space-time domain.

As discussed above, the grid function values of the source term f_i on the control volume Q_m^n as in Figure 2.1 are defined by

$$f(t_n + t, x_m + x) = (\delta_t - \sigma\triangle)\phi(t_n + t, x_m + x) \qquad (3.6)$$

such that

$$f_0 := f(t_n, x_m) = \phi_t(t_n, x_m) - \sigma\phi_{xx}(t_n, x_m) \qquad (3.7)$$

which is consistent with the strong form of the equation (2.1) at (t_n,x_m). Thus the source term is much more complicated and therefore needs an efficient quadrature approximation on the control volume to guarantee effective higher-order accurate discretizations of the equation.

We recast (3.2) for a one-step implicit time discretization of the equation on the control volume illustrated in Figure 2.1 by

$$\sum_{i=2}^{4} \alpha_i \phi_i^{n+1} - \sum_{i=6}^{8} \beta_i \phi_i^n = \sum_{i=2}^{4} w_i(\phi_i^{n+1} - \phi_0) + \sum_{i=6}^{8} w_i(\phi_i^n - \phi_0) + \sum_{i=0}^{8} v_i f_i. \qquad (3.8)$$

The assc

$$R_{kh} = \sum_{i=2}^{4} \alpha_i \phi_i^{n+1} - \sum_{i=6}^{8} \beta_i \phi_i^n - \sum_{i=2}^{4} w_i(\phi_i^{n+1} - \phi_0) - \sum_{i=6}^{8} w_i(\phi_i^n - \phi_0) - \sum_{i=0}^{8} v_i f_i \qquad (3.9)$$

where

$$w_0 = \sum_{i=1}^{8} w_i = 0, \quad \sum_{i=2}^{4} \alpha_i = \frac{1}{k}, \quad \sum_{i=6}^{8} \beta_i = \frac{1}{k}, \quad \sum_{i=0}^{8} v_i = 1 \qquad (3.10)$$

are enforced to ensure that the differential and integral operator properties of the equation are preserved through the optimal set of weights for a particular discretization.

By applying the Cauchy-Kovalevskaya procedure [23], the leading terms of the error expansion R_{kh} are reorganized in terms of the partial derivatives φ_t, φ_x, φ_{xt}, φ_{xx}, φ_{tt}, φ_{xtt}, φ_{xxt}, φ_{xxx}, f_t, f_x, f_{xt}, f_{xx}, f_{tt}, etc where their coefficients are functions of κ, h, σ, α_h, α_k and the quadrature weights. The optimal sets of weights $\{\alpha_i,\beta_i,w_i,v_i\}$ are then determined to eliminate the leading terms of error expansion.

4. A Family of One-Step Three-Point Discretizations

In this section, we present one-step three-point discretizations for the parabolic equation (3.8) based on constrained minimization of the local space-time equation error expansion.

To discretize $\int_{\partial \mathbf{Q}_m^n} \phi \cdot \eta_t \, dx$ implicitly about the centroid as indicated by the left side of (3.8), $\sum_{i=2}^{4} \alpha_i \phi_i^{n+1}$ is described as a weighted combination of φ_2, φ_3 and φ_4 at time t_{n+1} while $\sum_{i=6}^{8} \beta_i \phi_i^n$ is a weighted distribution of φ_6, φ_7 and φ_8 at time t_n. We then define a one-step implicit-time differencing of $\int_{\partial \mathbf{Q}_m^n} \phi \cdot \eta_t \, dx$ on the control volume in Figure 2.2 by

$$\sum_{\partial \mathbf{Q}_m^n t_{n+1}} \alpha_i \phi_i - \sum_{\partial \mathbf{Q}_m^n t_{n-1}} \beta_i \phi_i := \frac{\alpha_2(\phi_2 + \phi_4) + (1 - 2\alpha_2)\phi_3}{k} - \frac{\beta_6(\phi_6 + \phi_8) + (1 - 2\beta_6)\phi_7}{k} \tag{4.1}$$

where $0 \leq \alpha_i, \beta_i \leq 1$, $\sum \alpha_i = 1$, $\sum \beta_i = 1$, and the grid function values φ_6, φ_7 and φ_8 are within the domain of dependence of the centroid.

A one-step discretization of (3.1) using the stencil in Figure 2.1 may then be described based on (3.8) and (4.1) as

$$\frac{\mu_k(\phi_2 + \phi_4) + (1 - 2\mu_k)\phi_3}{k} - \frac{\mu_k(\phi_6 + \phi_8) + (1 - 2\mu_k)\phi_7}{k}$$
$$-\frac{\sigma\theta}{h^2}(\phi_2 + \phi_4 - 2\phi_3) - \frac{\sigma(1-\theta)}{h^2}(\phi_6 + \phi_8 - 2\phi_7) - \sum_{i=0}^{8} \beta_i f_i + R_{hk} \tag{4.2}$$

where

$$\beta_0 = 1 - 2\beta_5 - \frac{1}{3\alpha_k^2}, \quad \beta_1 = \beta_5,$$
$$\beta_2 = \beta_4 = -\frac{\sigma\, k}{12\alpha_h^2 \alpha_k h^2} + \frac{\sigma\, k(1-2\theta)}{12\alpha_h^2 \alpha_k^2 h^2} + \frac{\mu_k}{6\alpha_h^2 \alpha_k^2}, \tag{4.3}$$
$$\beta_6 = \beta_8 = \frac{\sigma\, k}{12\alpha_h^2 \alpha_k h^2} + \frac{\sigma\, k(1-2\theta)}{12\alpha_h^2 \alpha_k^2 h^2} + \frac{\mu_k}{6\alpha_h^2 \alpha_k^2}, \tag{4.4}$$
$$\beta_3 = \frac{1}{6\alpha_k^2} + \frac{\sigma\, k}{6\alpha_h^2 \alpha_k h^2} + \frac{\sigma\, k(1-2\theta)}{6\alpha_h^2 \alpha_k^2 h^2} - \frac{\mu_k}{3\alpha_h^2 \alpha_k^2}, \tag{4.5}$$
$$\beta_7 = \frac{1}{6\alpha_k^2} - \frac{\sigma\, k}{6\alpha_h^2 \alpha_k h^2} - \frac{\sigma\, k(1-2\theta)}{6\alpha_h^2 \alpha_k^2 h^2} - \frac{\mu_k}{3\alpha_h^2 \alpha_k^2}, \tag{4.6}$$

and R_{hk} as the residual error to be conditioned for a more uniform convergence of the resulting schemes. The parameters μ_k, θ, α_h, and α_k are to be determined to regulate the associated residual error R_{hk}, which is re-organized along a parabolic space-time curve

$$\sigma\, k = \kappa h^2 \tag{4.7}$$

by

$$\mathrm{R}_{hk} \approx T_2 h^2 + T_4 h^4 + T_6 h^6 + O(h^8) \tag{4.8}$$

with

$$T_2 = \frac{\sigma(12\mu_k - 1 + 6\kappa(1-2\theta))}{12}\frac{\partial^4\phi}{\partial x^4} - \frac{6\alpha_k^2(\beta_5\alpha_h^2 - \mu_k) + 2\kappa\theta(3\alpha_k^2 - 1) + \kappa + 2\mu_k - 6\mu_k\alpha_k^2}{6\alpha_k^2}\frac{\partial^2 f}{\partial x^2}$$

$$T_4 = -\frac{\sigma(1 - 20\mu_k + 30\kappa^2 + 15\kappa(2\theta-1))}{360}\frac{\partial^6\phi}{\partial x^6} + \frac{\kappa(2\theta-1)(\alpha_h^2-1) - 2\kappa^2 + 2\mu_k(1-\alpha_h^2)}{24}\frac{\partial^4 f}{\partial x^4}$$

$$T_6 = -\frac{1 - 56\mu_k - \sigma(420\kappa^3(2\theta-1) + 210\kappa^2(1-4\mu_k) + 28\kappa(2\theta-1))}{20160}\frac{\partial^8\phi}{\partial x^8} - \frac{\kappa^2(3 + 6\kappa(2\theta-1) - 2\alpha_h^2 - 12\mu_k)}{288}\frac{\partial^5 f}{\partial x^4\partial t} \frac{\kappa(30\kappa^2(1-2\theta) - \kappa(60\mu_k - 15) + 2 + 4\mu_k + 2\alpha_h^4(2\theta - 1 - 2\mu_k) + 2(1-2\theta))}{1440}\frac{\partial^6 f}{\partial x^6}$$

$$T_8 = \frac{\kappa^4(3 - 5\alpha_k^2)}{5760\sigma^4}\frac{\partial^4 f}{\partial t^4} + \frac{\kappa^4(5\alpha_k^2 - 3)}{1440\sigma^3}\frac{\partial^5 f}{\partial x^2\partial t^3} + \cdots .$$

The local diffusive rate within the computational domain, κ, which is also referred to as the numerical Fourier Number may be selected to control the resulting residual errors. According to Taylor's Theorem, the higher-order derivatives in (4.8) reflect the smoothness of the solution about the centroid. Therefore, for non-smooth data conditions [5] as well as for higher local accuracies, the remaining parameters κ, α_h, α_k, and β_5 may need to be determined to regulate the leading coefficients of the residual error in order to control φ_{xxxx}, f_{xx}, etc. and therefore improve local accuracies.

4.1. Stability and Accuracy Analyses

By Von Neumann stability analysis, the amplification factor, G, for the homogeneous version of the scheme (4.2) is determined as

$$G := \frac{1 + 4(\kappa\theta - \mu_k)\sin^2\left(k_m\frac{h}{2}\right) - 4\kappa\sin^2\left(k_m\frac{h}{2}\right)}{1 + 4(\kappa\theta - \mu_k)\sin^2\left(k_m\frac{h}{2}\right)}, = 1 - \frac{4\kappa\sin^2\left(k_m\frac{h}{2}\right)}{1 + 4(\kappa\theta - \mu_k)\sin^2\left(k_m\frac{h}{2}\right)} \tag{4.9}$$

where $\kappa = \sigma\frac{k}{h^2}$ and k_m is the wave number.

Clearly, any scheme with $\mu_k < \kappa\theta$ is implicit and unconditionally stable which includes the Backward Euler and the crank-Nicholson schemes while $\mu_k = \kappa\theta$ produces an explicit scheme as in the forward Euler scheme. Thus, there are several ways to come up with either an explicit scheme or an implicit scheme for

the parabolic equation (2.1). The key here should therefore depend on local accuracy performance which is connected to the functional nature of the leading coefficients of the residual error error (4.8).

On one hand, for the case of the implicit backward-Euler scheme with $\theta = 1$ and $\mu_k = 0$, the sinusoidal component of the numerator is eliminated rendering the scheme more preferable for non-smooth or sharp data conditions in the solution profile [5]. However, for $\frac{1}{2} < \theta \leq 1$ and $\mu_k = 0$, the coefficients of $\varphi^{(4)}(x)$, $\varphi^{(6)}(x)$, etc within the leading terms of the residual error stay increasingly negative and therefore anti-diffusive for any κ. Thus, the larger the value of κ, the higher the level of "pollution error" for such schemes.

On the other hand, the local expansion (3.9) and the leading coefficients of the residual error (4.8) offer alternative more locally accurate options.

4.2. Source Term Discretizations for Higher Accurate Second Order Schemes

In this section, we demonstrate how efficient source term discretizations may be constructed to achieve higher local accuracies and streamline convergence of computational errors. The derivatives of the local point-wise equation error

$$R_{ixjt} := \frac{\partial^p}{\partial x^i \partial t^j} \{\phi_t - \sigma\phi_{xx} - f\} \tag{4.10}$$

where $p = 0,1,2,3,\cdots$ and $i + j = p$, which may be factored into the h^2 term of the error expansion (4.8) for instance, are of the form

$$R_{2x0t} := \left(A_{2x}^k \phi_{xxt} - \sigma A_{2x}^h \phi_{xxxx} - A_{2x}^f f_{xx}\right)|_{(c_h, c_k)}, \tag{4.11}$$

and

$$R_{0x1t} := \left(A_{1t}^k \phi_{tt} - \sigma A_{1t}^h \phi_{xxt} - A_{1t}^f f_t\right)|_{(c_h, c_k)}, \tag{4.12}$$

By incorporating (4.10) into (4.8), the strategy is to determine the collocation weights for the source term with the objective to control and regulate the residual error. Thus, we determine the collocation weights to first eliminate the temporal derivative f_t as described in (4.12). A ratio parameter β_f whose value may be utilized for the spatial distribution of the local source characterized by f_{xx} to cancel out the error effects of φ_{xxxx} in the residual error as described in (4.11) is then introduced. That is, β_f is introduced and β_5 is determined in (4.8) such that

$$A_{2x}^f = \beta_f \sigma\, A_{2x}^h \quad \text{with} \quad A_{2x}^k = 0, \tag{4.13}$$

where

A For $\beta_f = 0$, f_{xx} is outrightly eliminated,

B The value of β_f may be determined for which the computational error achieves a minimum when the error contributions from φ_{xxxx} are cancelled out by f_{xx},

C The β_f may be chosen to regulate the natural convergence of the local point-wise equation errors as described in (4.10) as much as possible.

Thus, β_0 and β_5 in (4.3) may then be determined as

$$\beta_0 = 1 + \frac{2\mu_k}{3\alpha_k^2\alpha_h^2} - \frac{1}{3\alpha_k^2} - \frac{2\mu_k}{\alpha_h^2} + \frac{k(2\theta-1)}{\alpha_h^2 h^2} + \frac{k(1-2\theta)}{3\alpha_h^2\alpha_k^2 h^2} + \frac{\mu_k(2\alpha_k^2-1)}{3\alpha_h^2\alpha_k^2}$$
$$+\beta_f\sigma\left(\frac{k(1-2\theta)}{\alpha_h^2 h^2} + \frac{(12\mu_k-1)}{6\alpha_h^2}\right)$$
$$\beta_5 = \frac{k(1-2\theta)}{2\alpha_h^2 h^2} + \frac{k(1-2\theta)}{6\alpha_h^2\alpha_k^2 h^2} + \frac{\mu_k(3\alpha_k^2-1)}{3\alpha_h^2\alpha_k^2} + \beta_f\sigma\left(\frac{k(2\theta-1)}{2\alpha_h^2 h^2} + \frac{(1-12\mu_k)}{12\alpha_h^2}\right)$$

in order to match the coefficient of f_{xx} with that of φ_{xxxx} in (4.8).

Consequently, T_2 in (4.8) becomes

$$T_2 = \frac{\sigma(12\mu_k - 1 + 6\kappa(1-2\theta))}{12}\left(\frac{\partial^4\phi}{\partial x^4} + \beta_f\frac{\partial^2 f}{\partial x^2}\right) \qquad (4.14)$$

and T_4 is modified as

$$T_4 = -\frac{\sigma(1-20\mu_k+30\kappa^2+15\kappa(2\theta-1))}{360}\frac{\partial^6\phi}{\partial x^6}$$
$$+\sigma\beta_f\alpha_h^2\left(\frac{k(1-2\theta)}{24h^2} + \frac{12\mu_k-1}{144}\right)\frac{\partial^4 f}{\partial x^4}$$
$$+\left(\frac{\kappa(2\theta-1)(\alpha_h^2-1) - 2\kappa^2 + 2\mu_k(1-\alpha_h^2)}{24}\right)\frac{\partial^4 f}{\partial x^4}. \qquad (4.15)$$

To allow for the capacity to also regulate T_4, additional points for the source term may be needed to control the approximation of $\frac{\partial^6\phi}{\partial x^6}$ even for second order schemes to achieve higher local accuracies. In particular, for four additional coordinate directional points defined by

$$f_{1a} := f(x_m + \pi_h h, t_n), \qquad f_{5a} := f(x_m - \pi_h h, t_n),$$
$$f_{3a} := f(x_m, t_n + \alpha_{k_2} k/2), \qquad f_{7a} := f(x_m, t_n - \alpha_{k_2} k/2), \qquad (4.16)$$

the coefficient of $\frac{\partial^4 f}{\partial x^4}$ in (4.20) becomes

$$A_{4x}^f = \beta_f\frac{6\sigma^2\pi_h^2 k(1-2\theta) + \sigma\pi_h^2(12\mu_k-1)}{144h^2} + \beta_\pi\frac{\pi_h^2(\alpha_h^2-\pi_h^2)}{12} + \theta\frac{\sigma\, k(\alpha_h^2-1)}{12h^2}$$
$$+\mu_k\frac{1-\alpha_h^2}{12} + \frac{\sigma\, k(1-\alpha_h^2)}{24h^2} - \frac{\sigma^2\, k^2}{12h^4}$$
$$12$$

where $\pi_h \neq \alpha_h$ and β_π is the collocation weight for f_{1a} and f_{5a} in (4.16). Instead of outright elimination of $\frac{\partial^4 f}{\partial x^4}$, β_π may be determined as described in (4.13) by

$$A_{4x}^f = \beta_{\pi_f}\sigma\, A_{4x}^h \quad \text{with} \quad A_{4x}^k = 0, \qquad (4.17)$$

where a $\beta_{\pi f}$ is the ratio value at which $\frac{\partial^4 f}{\partial x^4}$ cancels the error effects of $\frac{\partial^6\phi}{\partial x^6}$ from the computational error. Clearly, the error terms (4.14) and (4.15) offer two approaches for local accuracy improvements. One obvious approach is through a higher-order accuracy by choosing θ and μ_k to eliminate $T2$ in which case the local solutions φ_is are manipulated as discussed in the next section. The other approach is through the manipulation of the local source terms f_is.

4.3. Implicit Fourth-order Accurate Discretizations

As described in the previous section, one way for a more accurate discretization of (3.1) is to choose θ and μ_k to eliminate $T2$. Using a finite volume quadrature differencing for $\int_{\partial Q_m^n} \phi \cdot \eta_t \, dx$ between the times t_n and t_{n+1} as described in (4.1), a three-point one-step implicit discretization of (3.1) obtained by determining $\theta = \frac{1}{2}$ and $\mu_k = \frac{1}{12}$ to eliminate $T2$ is given as

$$\frac{10\phi_3 + \phi_2 + \phi_4}{12k} - \frac{10\phi_7 + \phi_6 + \phi_8}{12k} = \sigma \frac{\phi_2 + \phi_4 - 2\phi_3 + \phi_6 + \phi_8 - 2\phi_7}{2h^2}$$
$$+ f_0 + \frac{f_3 + f_7 - 2f_0}{6\alpha_k^2} + \frac{f_5 + f_5 - 2f_0}{12\alpha_h^2} + \sigma k \frac{(f_6 + f_8 - 2f_7) - (f_2 + f_4 - 2f_3)}{12\alpha_h^2 \alpha_k h^2}$$
$$+ \frac{(f_6 + f_8 - 2f_7) - 2(f_1 + f_5 - 2f_0) + (f_2 + f_4 - 2f_3)}{72\alpha_h^2 \alpha_k^2} \qquad (4.18)$$

where α_h and α_k may be chosen to regulate the rate of convergence by matching the leading coefficients of the error as discussed above. The amplification factor for the homogeneous part of the scheme is given as

$$G = \frac{1 - \left(2\kappa + \frac{1}{3}\right) \sin^2 \left(k_m \frac{h}{2}\right)}{1 + \left(2\kappa - \frac{1}{3}\right) \sin^2 \left(k_m \frac{h}{2}\right)} \qquad (4.19)$$

and therefore unconditionally stable [19]. The resulting residual error E_{hk} is reorganized as

$$\mathrm{E}_{hk} \approx T_4 h^4 + T_6 h^6 + T_8 h^8 + O(h^{10}) \qquad (4.20)$$

with

$$T_4 = \frac{\sigma(1 - 20\kappa^2)}{240} \frac{\partial^6 \phi}{\partial x^6} + \frac{1 - \alpha_h^2 - 12\kappa^2}{144} \frac{\partial^4 f}{\partial x^4}$$
$$T_6 = \frac{\sigma(11 - 420\kappa^2)}{60480} \frac{\partial^8 \phi}{\partial x^8} + \frac{(14 - 14\alpha_h^4 - 420\kappa^2)}{60480} \frac{\partial^6 f}{\partial x^6} + \frac{\kappa^2(\alpha_h^2 - 1)}{144\sigma} \frac{\partial^5 f}{\partial x^4 \partial t}$$
$$T_8 = \frac{\sigma(13 - 7560\kappa^4 - 210\kappa^2)}{3628800} \frac{\partial^8 \phi}{\partial x^8} + \frac{\kappa^4(3 - 5\alpha_k^2)}{5760\sigma^4} \frac{\partial^4 f}{\partial t^4} + \frac{\kappa^2(5\alpha_k^2 - 3)}{1440\sigma^3} \frac{\partial^5 f}{\partial x^2 \partial t^3}$$
$$+ \cdots$$

where α_k and α_h are to be determined.

For the collocation point value of $\alpha_h = 1$, the leading coefficient of f_{xxxx} in (4.20) puts a constraint on the size of κ [19] for local accuracies and computational convergence. This stiffness constraint may be eased with a sub-grid value of $\alpha_h \leq \frac{\sqrt{10}}{5}$ which creates a point-wise equation error coefficient ratios for $\frac{\partial^6 \phi}{\partial x^6}$ and $\frac{\partial^4 f}{\partial x^4}$. That is, a sub-grid point value of $\alpha_h = \frac{\sqrt{10}}{5}$ leads to coefficient ratios in the leading term of the residual error that matches the point-wise equation error about the centriod (4.10) and therefore provides for a more uniform convergence independent of κ as resolution is refined.

As discussed in [19], one way for improved local accuracy is a two-step method where the discretization of the diffusion term includes solution values at the centroid time level and uses a nine-point stencil on the

space-time domain in one spatial dimension. On the other hand as discussed above for the source term discretization, additional collocation points may be utilized to reduce or eliminate the effects of $\frac{\partial^6 \phi}{\partial x^6}$ on computational errors. In particular, for four additional symmetric points about the centroid defined by

$$f_{2a} := f(x_m + \pi_h h, t_n + \alpha_k k/2), \qquad f_{4a} := f(x_m - \pi_h h, t_n + \alpha_k k/2),$$
$$f_{8a} := f(x_m + \pi_h h, t_n - \alpha_k k/2), \qquad f_{6a} := f(x_m - \pi_h h, t_n - \alpha_k k/2), \qquad (4.21)$$

the coefficient of $\frac{\partial^4 f}{\partial x^4}$ in (4.20) becomes

$$\frac{24\pi_h^2 \beta_{\pi_h}(\alpha_h^2 - \pi_h^2) + 1 - \alpha_h^2 - 12\kappa^2}{144} \qquad (4.22)$$

where $\pi_h \neq \alpha_h$ and $\beta_{\pi h}$ is the collocation weight. Instead of outright elimination of $\frac{\partial^4 f}{\partial x^4}$, β_{π_h} may be parameterized as

$$\beta_{\pi_h} = \frac{60\kappa^2(1 - \beta_{\pi_f}) + 3\beta_{\pi_f} + 5(\alpha_h^2 - 1)}{120\pi_h^2(\alpha_h^2 - \pi_h^2)} \qquad (4.23)$$

where a $\beta_{\pi f}$ may be determined for $\frac{\partial^4 f}{\partial x^4}$ to reduce the effect of $\frac{\partial^6 \phi}{\partial x^6}$ on computational error.

5. Numerical Experiments. To demonstrate the effectiveness of the method for developing new higher-order efficient schemes for (2.1), we present some of the results of our tests to show accuracy improvements and associated uniform convergence rates.

The *p*−norm of the grid function error (global) on Ω at time *T*, is defined as

$$\|u - \phi\|_p = \left(h \sum_{i=0}^{N} |u(x_i, T) - \phi(x_i, T)|^p \right)^{1/p} \qquad (5.1)$$

where *u*(*x*,*t*) is the exact solution at time *t* and *φ*(*x*,*t*) is the space-time numerical approximation of *u*(*x*,*t*) at time *t*. Thus, *φ*(*x*,*T*) is the numerical solution of the equation on Ω at the end of time integration based on a spatial resolution *h*.

Consider the error e_T based on a spatial resolution of *h*, measured at the end of a time integration *T* with the L^∞ norm Ω according to

$$e_T(h) = \|u - \phi\|_{L^\infty} = Ch^r + o(h^r) \quad \text{as h} \to 0,$$

where *C* is independent of *h*. If *h* is sufficiently small, then

$$e_T(h) \approx Ch^r, \text{ and } R(h) = \frac{e(h)}{e(\frac{h}{2})} \approx 2^r$$

where *r* is the order of accuracy or the convergence rate.

Example 1. As a first example, consider the exact solution to (2.1) to be

$$u(x,t) = \frac{1}{2}\{\cos(t - \pi x) + \cos(t + \pi x)\} \text{ with } \quad \Omega_T = (0, T] \times [0, 1]. \qquad (5.2)$$

With σ = 1, the initial distribution as $u_0(x)$ = cosπx, and the boundary conditions as $g(0,t) = \cos t$ and $g(1,t) = -\cos t$, the source term is determined as

$$f(x,t) = \pi^2 \cos t \cos \pi x - \sin t \cos \pi x.$$

Example 2. For a second example, consider the exact solution with $\sigma = 1$ to be

$$u(x,t) = \sin(\omega x) \exp(-\beta^2 t) \text{ with } \quad \Omega_T = (0,T] \times [0,1] \tag{5.3}$$

With the initial distribution as $u_0(x) = \sin(\omega x)$, and the boundary conditions as $g(0,t) = 0$ and $g(1,t) = \sin(\omega) \exp(-\beta^2 t)$, the source term is determined as

$$f(x,t) = (\omega^2 - \beta^2) \sin(\omega x) \exp(-\beta^2 t).$$

Example 3. As a third example, consider the exact solution with $\sigma = 1$ as

$$u(x,t) = \frac{1}{2}\{1 + \tanh(\gamma \cos(2\pi t))\} \sin(\kappa x \cos\phi) \text{ with } \quad \Omega_T = (0,T] \times [0,1] \tag{5.4}$$

With the initial distribution as $u_0(x) = u(x,0)$ and the boundary conditions as $g(0,t) = 0$ and $g(1,t) = u(1,t)$, the source term is similarly determined as

$$\begin{aligned} f(x,t) = {} & (\tanh(\gamma \cos(2\pi t))^2 - 1)\gamma \sin(2\pi t)\pi \sin(\kappa x \cos(\phi)) \\ & + 1/2\sigma(1 + \tanh(\gamma \cos(2\pi t))) \sin(\kappa x \cos(\phi))\kappa^2 \cos(\phi)^2. \end{aligned}$$

With T = 2, we examine accuracy improvements and the higher-order convergence rates of the new schemes in the numerical experiments below.

Experiment 1. The amplification factor (4.9) clearly reveals that an implicit scheme is guaranteed with $\mu_k < \kappa$. Therefore, the objective in this experiment is to demonstrate how the pairings of $0 \leq \mu_k < 1/2$ with $0 \leq \theta \leq 1$ affect local accuracy. We consider situations when $\mu_k \neq 1/12$ and $\theta \neq 1/2$ in which cases the discretizations are second order accurate in space.

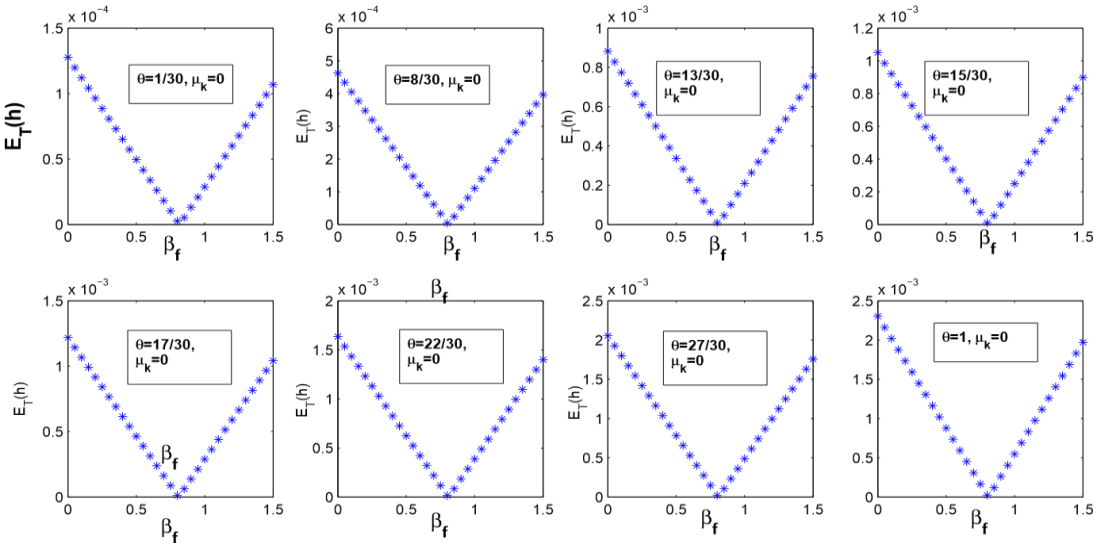

FIG. 5.1. *Error plots are for different source term discretizations as* β_f *is varied from* $\beta_f = 0$ *to* $\beta_f = 1.5$ *with* $h = 1/8$ *and* $\mu_k = 0$. *The minimum point shows the value of* β_f *at which* $\frac{\partial^2 f}{\partial x^2} + \beta_f \frac{\partial^4 \phi}{\partial x^4} = 0$ *for* $\kappa = 1/5$

Figure 5.1 shows that when μ_k is small as in $\mu_k = 0$, smaller values of θ produce better local accuracies and accuracy decreases as θ is increased.

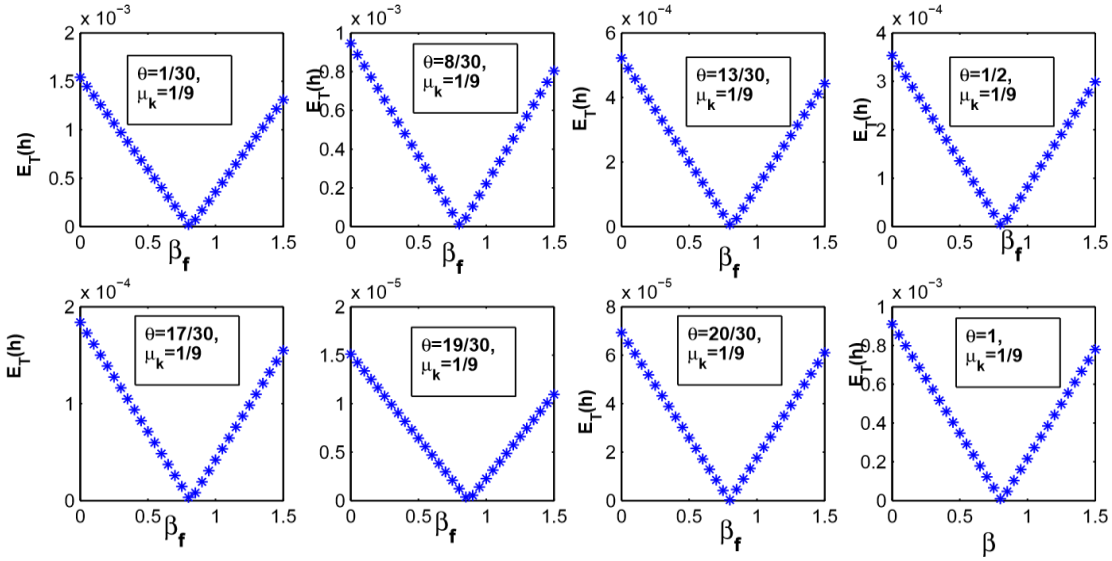

FIG. 5.2. *Error plots are for different source term discretizations as* β_f *is varied from* $\beta_f = 0$ *to* $\beta_f = 1.5$ *with* $h = 1/8$ *and* $\mu_k = 1/9$. *The minimum point shows the value of* β_f *at which* $\frac{\partial^2 f}{\partial x^2} + \beta_f \frac{\partial^4 \phi}{\partial x^4} = 0$ *for* $\kappa = 1/5$

In Figure 5.2 with $\mu_k = 1/9$, lowest errors are achieved when θ ia about 2/3.

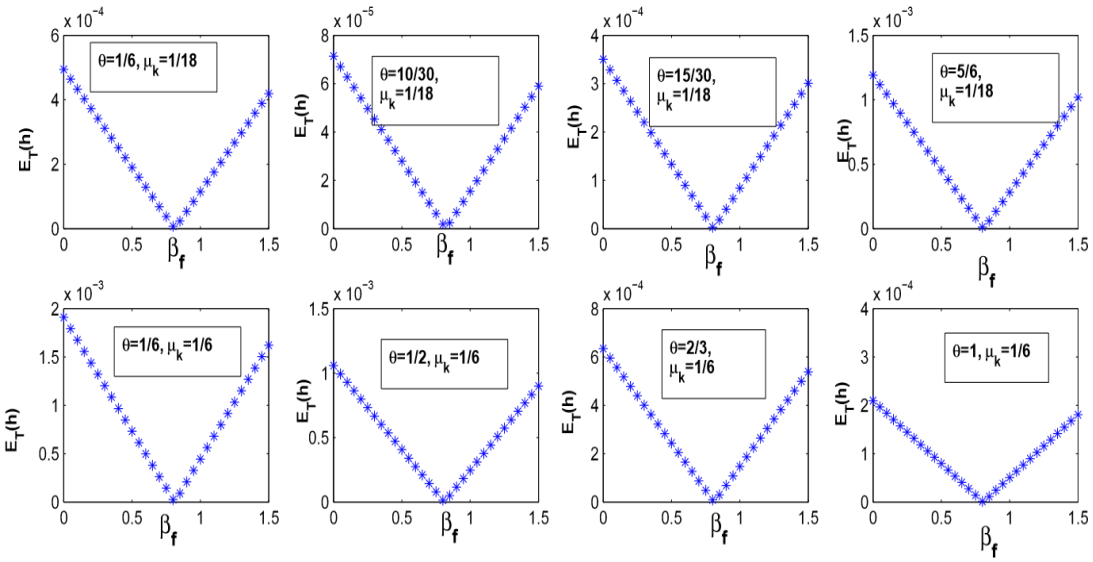

FIG. 5.3. *Error plots are for different source term discretizations as* β_f *is varied from* $\beta_f = 0$ *to* $\beta_f = 1.5$ *with* $h = 1/8$ *and* $\mu_k = 1/18$ *and* $\mu_k = 1/6$. *The minimum point shows the value of* β_f *at which* $\frac{\partial^2 f}{\partial x^2} + \beta_f \frac{\partial^4 \phi}{\partial x^4} = 0$ *for* $\kappa = 1/5$

In Figure 5.3 with $\mu_k = 1/18$, lowest errors are achieved when θ ia about 1/3 but for $\mu_k = 1/6$ lowest errors are achieved with $\theta = 1$. Thus, as θ is increased μ_k must also increase and vice versa to create second order discretizations that produce higher local accuracies.

Experiment 2. The purpose of this experiment is first to demonstrate the levels of local accuracy improvements that may be achieved with Crank-Nicholson scheme for different source term discretizations. In Table 5.1, column 1 with CN refers the errors for the traditional scheme with source term collocation as $\frac{1}{2}(f_3 + f_7)$.

Column 2 with $\beta_f = \beta_{\pi f} = 1$ refers to the source term discretization where residual error (4.8) has been regulated by factoring in the local equation error residuals as described in (4.13) for the $O(h^2)$ term and in (4.17) for the $O(h^4)$ term. Column 3 with $\beta_f = -1.95$ refers to the source term discretization where only the $O(h^2)$ term of the residual error is regulated by determining the best value of β_f for the best results based on the relationship between the particular solution and the source term.

TABLE 5.1
Grid refinement analysis for Example 1 with Crank-Nicholson discretization for ϕ and different source term discretizations with $\kappa = 1/5$

h	k	CN $\|u-\phi\|_{L_\infty}$	cvge. rate	$\beta_f = \beta_{\pi_f} = 1$ $\|u-\phi\|_{L_\infty}$	cvge. rate	$\beta_f = -1.95$ $\|u-\phi\|_{L_\infty}$	cvge. rate
$\frac{1}{8}$	$\frac{h^2}{5}$	$1.049e^{-3}$		$2.485e^{-4}$		$3.564e^{-3}$	
$\frac{1}{16}$	$\frac{2h^2}{5}$	$2.614e^{-4}$	2.00	$6.173e^{-5}$	2.01	$7.622e^{-4}$	2.23
$\frac{1}{32}$	$\frac{4h^2}{5}$	$6.646e^{-5}$	1.98	$1.566e^{-5}$	1.98	$1.282e^{-4}$	2.57
$\frac{1}{64}$	$\frac{8h^2}{5}$	$1.661e^{-5}$	2.00	$3.913e^{-6}$	2.00	$8.285e^{-7}$	7.28

Results in Table 5.1 show that local accuracies may be improved significantly by utilizing the source term collocations where the residual error as determined in (4.8) is regulated over the traditional Crank-Nicholson collocation of the source term. Additionally, in Figure 5.4, the error distribution $e_T(h)$ for varying β_fs clearly show that a minimum may be achieved at which cancels $\frac{\partial^2 f}{\partial x^2}$ error contribution of without regulating the $O(h^4)$ term of the error. However, when the $O(h^4)$ term of the error is regulated with $\beta_{\pi f} = 1$ as described in (4.17) and illustrated by Figure 5.5, uniform convergence is demonstrated with consistent numerical determinations of β_f.

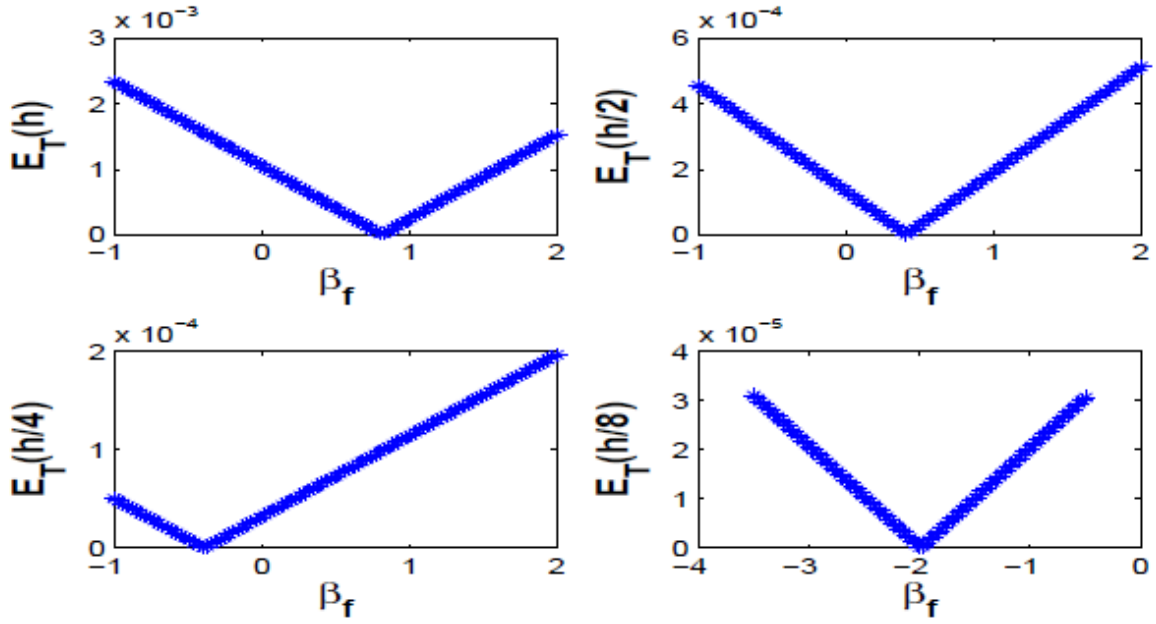

FIG. 5.4. *Error plots are for the Crank-Nicholson discretization of ϕ with varying source term collocations based on β_f for $h = 1/8$. The $O(h^4)$ term of the error is not regulated by β_{π_f} as described in (4.17).*

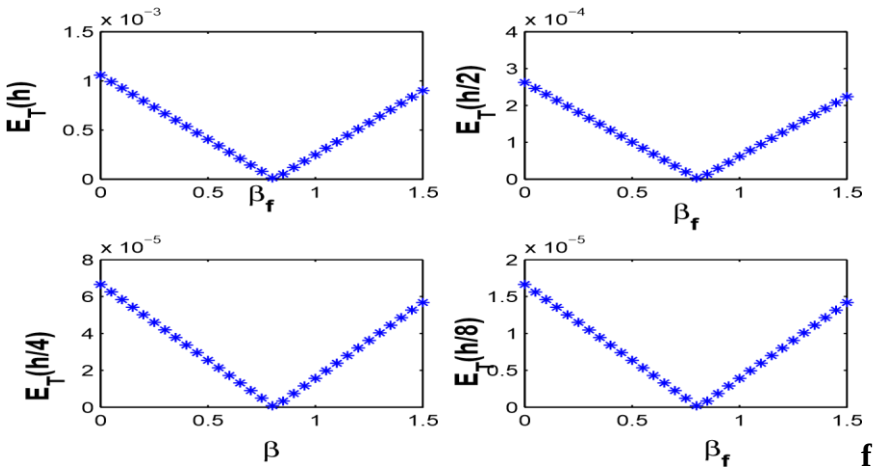

Fig. 5.5. *Error plots are for the Crank-Nicholson discretization of φ with varying source term collocations based on β_f for h = 1/8. The $O(h^4)$ term of the error is regulated with $\beta\pi_f = 1$ as described in (4.17).*

Experiment 3. In this experiment we demonstrate local accuracy improvements for the Backward Euler scheme with different discretizations for the source term.

In Table 5.2, column 1 refers the errors for determining the source term collocations $\partial^2 f$ to eliminate $\partial x 2$ from the residual error.

Column 2 with $\beta_f = \beta_{\pi f} = 1$ refers to the source term discretization where residual error (4.8) has been regulated by factoring in the local equation error residuals as described in (4.13) for the $O(h^2)$ term and in (4.17) for the $O(h^4)$ term. Column 3 with $\beta_f = -1.95$ refers to the source term discretization where only the $O(h^2)$ term of the residual error is regulated by determining the value of β_f for the best results based on the relationship between the solution and the source term.

TABLE 5.2

Grid refinement analysis for Example 1 with Crank-Nicholson discretization for ϕ and different source term discretizations with $\kappa = 1/5$

h	k	$\beta_f = 0$ $\|u-\phi\|_{L_\infty}$	cvge. rate	$\beta_f = \beta_{\pi_f} = 1$ $\|u-\phi\|_{L_\infty}$	cvge. rate	$\beta_f = 3/10$ $\|u-\phi\|_{L_\infty}$	cvge. rate
$\frac{1}{8}$	$\frac{h^2}{5}$	$2.291e^{-3}$		$5.465e^{-4}$		$1.443e^{-3}$	
$\frac{1}{16}$	$\frac{2h^2}{5}$	$6.286e^{-4}$	1.87	$2.106e^{-4}$	1.38	$2.999e^{-4}$	2.27
$\frac{1}{32}$	$\frac{4h^2}{5}$	$1.880e^{-4}$	1.74	$9.126e^{-5}$	1.21	$4.510e^{-5}$	2.73
$\frac{1}{64}$	$\frac{8h^2}{5}$	$6.099e^{-5}$	1.62	$4.171e^{-5}$	1.13	$4.448e^{-6}$	3.38

Results in Table 5.2 clearly show that the weighted quadrature approximation for the source term, $\sum v_i f_i$, has been effective since the implicit backward Euler scheme can be made to achieve higher local accuracies at par with the Crank Nicholson scheme. By choosing $\beta_f = 0$ to eliminate $\frac{\partial^2 f}{\partial x^2}$ as in the first column, accuracy performance is slightly below the Crank-Nicholson discretization. However, it performs at par with $\beta_f = 3/14$ and outperforms with $\beta_f = 3/10$ as demonstrated in the third column. Additionally, choosing β_f

= $\beta_{\pi f}$ = 1 to regulate the equation error expansion ensures that convergence of the scheme stays uniform and more accurate at lower resolutions.

Experiment 4. In this experiment, we demonstrate the computational convergence of the fourth-order scheme (4.18) for the traditional source term collocation with $\alpha_h = 1$. Since the leading coefficients of the residual errors (4.20) is quadratic in κ, relatively large values of κ creates a 'pollution' effect on accuracy and affects the convergence rate. Results for example 1, example 2, and example 3 are shown in Tables 5.3, 5.4, 5.4 respectively.

TABLE 5.3
Grid refinement analysis for Example 1 with the Implicit Fourth-Order Scheme (4.18)

h	k	$\kappa = 1/5$ $\|u-\phi\|_{L_\infty}$	cvge. rate	$\kappa = 1/20$ $\|u-\phi\|_{L_\infty}$	cvge. rate	$\kappa = 1/40$ $\|u-\phi\|_{L_\infty}$	cvge. rate
$\frac{1}{8}$	$\frac{h^2}{\kappa}$	$9.631e^{-6}$		$8.197e^{-6}$		$8.125e^{-6}$	
$\frac{1}{16}$	$\frac{2h^2}{\kappa}$	$8.864e^{-7}$	3.44	$5.280e^{-7}$	3.96	$5.101e^{-7}$	3.99
$\frac{1}{32}$	$\frac{4h^2}{\kappa}$	$1.292e^{-7}$	2.78	$3.810e^{-8}$	3.79	$3.355e^{-8}$	3.93
$\frac{1}{64}$	$\frac{8h^2}{\kappa}$	$2.629e^{-8}$	2.30	$3.519e^{-9}$	3.44	$2.381e^{-9}$	3.82

Results from Table 5.3 show that the size of κ determines the uniformity of the rate of computational convergence of the scheme (4.18). As κ is lowered from 1⁄5 to 1⁄20 and then 1⁄40, local accuracies improved and the computational convergence improves toward a robust fourth-order rate.

TABLE 5.4
Grid refinement analysis for Example 2 with the Implicit Fourth-Order Scheme (4.18)

h	k	$\kappa = 1/20$ $\|u-\phi\|_{L_\infty}$	cvge. rate	$\kappa = 1/30$ $\|u-\phi\|_{L_\infty}$	cvge. rate	$\kappa = 1/40$ $\|u-\phi\|_{L_\infty}$	cvge. rate
$\frac{1}{8}$	$\frac{h^2}{\kappa}$	$2.004e^{-9}$		$2.048e^{-9}$		$2.063e^{-9}$	
$\frac{1}{16}$	$\frac{2h^2}{\kappa}$	$1.099e^{-10}$	4.19	$1.210e^{-10}$	4.08	$1.248e^{-10}$	4.04
$\frac{1}{32}$	$\frac{4h^2}{\kappa}$	$3.153e^{-12}$	5.12	$5.904e^{-12}$	4.36	$6.867e^{-12}$	4.18
$\frac{1}{64}$	$\frac{8h^2}{\kappa}$	$7.232e^{-13}$	2.11	$4.385e^{-14}$	7.07	$1.971e^{-13}$	5.12

From Table 5.4, the convergence rate for scheme (4.18) with example 2 tends toward uniformity as κ is decreased from 1⁄20 to 1⁄30 and then 1⁄40.

TABLE 5.5
Grid refinement analysis for Example 3 with the Implicit Fourth-Order Scheme (4.18)

h	k	$\kappa = 1/5$ $\|u-\phi\|_{L_\infty}$	cvge. rate	$\kappa = 1/20$ $\|u-\phi\|_{L_\infty}$	cvge. rate	$\kappa = 1/40$ $\|u-\phi\|_{L_\infty}$	cvge. rate
$\frac{1}{8}$	$\frac{h^2}{\kappa}$	$9.198e^{-3}$		$9.195e^{-3}$		$9.195e^{-3}$	
$\frac{1}{16}$	$\frac{2h^2}{\kappa}$	$6.234e^{-4}$	3.88	$6.222e^{-4}$	3.89	$6.222e^{-4}$	3.89
$\frac{1}{32}$	$\frac{4h^2}{\kappa}$	$3.877e^{-5}$	4.01	$3.849e^{-5}$	4.02	$3.847e^{-5}$	4.02
$\frac{1}{64}$	$\frac{8h^2}{\kappa}$	$2.473e^{-6}$	3.97	$2.403e^{-6}$	4.00	$2.399e^{-6}$	4.00

Results from Table 5.5 for Example 3 support the notion that while it is desirable to have large time step sizes, consistency of results of higher-order schemes like (4.18) suffer from pollution effects for larger time step sizes.

Experiment 5. The objective of this experiment is to demonstrate the robustness of the computational convergence for the three-point quadrature scheme (4.18) with sub-grid collocations for the source term. From the leading coefficients in (4.20), a value of $\alpha_h = \sqrt{2/}$ 5 creates convergence ratios with $\beta_f = 1$ as in (4.13) ensuring

that $\frac{\partial^4 f}{\partial x^4}$ and $\frac{\partial^6 \phi}{\partial x^6}$ converge at the same rate as the fourth-order derivative of the local equation errors about each centroid.

TABLE 5.6
Grid refinement analysis for Example 1 with the Implicit Fourth-Order Scheme (4.18) for $\kappa = 1/40$

h	k	$\alpha_h = 0.61$ $\|u-\phi\|_{L_\infty}$	cvge. rate	$\alpha_h = \sqrt{2/5}$ $\|u-\phi\|_{L_\infty}$	cvge. rate	$\alpha_h = 0.67$ $\|u-\phi\|_{L_\infty}$	cvge. rate
$\frac{1}{8}$	$\frac{h^2}{\kappa}$	$2.362e^{-6}$		$1.894e^{-6}$		$1.076e^{-6}$	
$\frac{1}{16}$	$\frac{2h^2}{\kappa}$	$1.426e^{-7}$	4.05	$1.136e^{-7}$	4.06	$6.276e^{-8}$	4.10
$\frac{1}{32}$	$\frac{4h^2}{\kappa}$	$7.915e^{-9}$	4.17	$6.072e^{-9}$	4.23	$2.842e^{-9}$	4.46
$\frac{1}{64}$	$\frac{8h^2}{\kappa}$	$2.100e^{-10}$	5.24	$9.488e^{-11}$	6.00	$1.070e^{-10}$	4.73

Results from Tables 5.3 and 5.6 show that utilizing sub-grid collocations for the source term has been effective for improved local accuracies as well as the convergence rates.

TABLE 5.7
Grid refinement analysis for Example 2 with the Implicit fourth-order Scheme (4.18) for $\kappa = 1/40$

h	k	$\alpha_h = 0.61$ $\|u-\phi\|_{L_\infty}$	cvge. rate	$\alpha_h = \sqrt{2/5}$ $\|u-\phi\|_{L_\infty}$	cvge. rate	$\alpha_h = 0.67$ $\|u-\phi\|_{L_\infty}$	cvge. rate
$\frac{1}{8}$	$\frac{h^2}{\kappa}$	$1.549e^{-9}$		$1.572e^{-9}$		$1.612e^{-9}$	
$\frac{1}{16}$	$\frac{2h^2}{\kappa}$	$9.277e^{-7}$	4.06	$9.419e^{-11}$	4.06	$9.669e^{-11}$	4.06
$\frac{1}{32}$	$\frac{4h^2}{\kappa}$	$4.864e^{-12}$	4.25	$4.953e^{-12}$	4.25	$5.109e^{-12}$	4.24
$\frac{1}{64}$	$\frac{8h^2}{\kappa}$	$7.187e^{-14}$	6.08	$7.743e^{-14}$	6.00	$8.718e^{-14}$	5.87

Again, results from Tables 5.4 and 5.7 show that subgrid collocations for the source term has been effective for improved local accuracies and a more uniform computational convergence.

TABLE 5.8
Grid refinement analysis for Example 3 with the Implicit fourth-order Scheme (4.18) for $\kappa = 1/25$

h	k	$\alpha_h = 0.61$ $\|u-\phi\|_{L_\infty}$	cvge. rate	$\alpha_h = \sqrt{2/5}$ $\|u-\phi\|_{L_\infty}$	cvge. rate	$\alpha_h = 0.67$ $\|u-\phi\|_{L_\infty}$	cvge. rate
$\frac{1}{8}$	$\frac{h^2}{\kappa}$	$4.021e^{-4}$		$4.830e^{-5}$		$4.034e^{-4}$	
$\frac{1}{16}$	$\frac{2h^2}{\kappa}$	$2.879e^{-5}$	3.80	$1.o122e^{-6}$	5.43	$5.137e^{-5}$	3.97
$\frac{1}{32}$	$\frac{4h^2}{\kappa}$	$1.794e^{-6}$	4.00	$2.824e^{-8}$	5.31	$3.140e^{-6}$	4.03
$\frac{1}{64}$	$\frac{8h^2}{\kappa}$	$1.099e^{-7}$	4.03	$2.522e^{-9}$	3.49	$1.973e^{-7}$	3.99

Experiment 6. The objective of this experiment is to show that local accuracies may be further improved not only through a two-step method but also by reconfiguring the weighted quadrature approximation $\sum v_i f_i$ for (4.18) to include additional sub-grid points (4.23) to offset some of the effects of $\frac{\partial^6 \phi}{\partial x^6}$ on computational errors.

TABLE 5.9
Grid refinement analysis for the Implicit fourth-order Scheme (4.18) for $\alpha_h = 67/100$ *and* $\pi_h = 61/100$ *for Example* 1

h	k	$\kappa = 1/15$ $\beta_{\pi_f} = 2.00$ $\|u-\phi\|_{L_\infty}$	cvge. rate	$\kappa = 1/25$ $\beta_{\pi_f} = 1.20$ $\|u-\phi\|_{L_\infty}$	cvge. rate	$\kappa = 1/40$ $\beta_{\pi_f} = 0.95$ $\|u-\phi\|_{L_\infty}$	cvge. rate
$\frac{1}{8}$	$\frac{h^2}{\kappa}$	$1.090e^{-5}$		$3.803e^{-6}$		$1.399e^{-6}$	
$\frac{1}{16}$	$\frac{2h^2}{\kappa}$	$6.546e^{-7}$	4.08	$2.251e^{-7}$	4.08	$8.280e^{-8}$	4.08
$\frac{1}{32}$	$\frac{4h^2}{\kappa}$	$3.290e^{-8}$	4.29	$1.138e^{-8}$	4.31	$4.115e^{-9}$	4.33
$\frac{1}{64}$	$\frac{8h^2}{\kappa}$	$3.687e^{-11}$	9.80	$1.830e^{-11}$	9.28	$2.742e^{-11}$	7.23

Again, the results in Tables 5.3, 5.6 and 5.9 demonstrate very robust convergence rates for the scheme(4.18)

TABLE 5.10
Grid refinement analysis for the Implicit fourth-order Scheme (4.18) for $\alpha_h = 67/100$ *and* $\pi_h = 61/100$ *for Example* 3

h	k	$\kappa = 1/10$ $\beta_{\pi_h} = 0.9$ $\|u-\phi\|_{L_\infty}$	cvge. rate	$\kappa = 1/25$ $\beta_{\pi_h} = 1$ $\|u-\phi\|_{L_\infty}$	cvge. rate	$\kappa = 1/40$ $\beta_{\pi_h} = 1$ $\|u-\phi\|_{L_\infty}$	cvge. rate
$\frac{1}{8}$	$\frac{h^2}{\kappa}$	$7.901e^{-4}$		$4.819e^{-5}$		$4.841e^{-5}$	
$\frac{1}{16}$	$\frac{2h^2}{\kappa}$	$5.068e^{-5}$	3.96	$1.121e^{-6}$	5.43	$1.172e^{-6}$	4.08
$\frac{1}{32}$	$\frac{4h^2}{\kappa}$	$3.146e^{-6}$	4.01	$2.822e^{-8}$	5.31	$4.088e^{-8}$	4.84
$\frac{1}{64}$	$\frac{8h^2}{\kappa}$	$2.096e^{-7}$	3.91	$2.522e^{-9}$	3.48	$6.368e^{-10}$	6.00

As demonstrated above in Experiments 4 and 6, uniform fourth-order computational convergence requires κ to be small to avoid 'pollution' errors.

6. Extensions

In a two-dimensional extension, the space-time domain is three-dimensional where the control volume is the cube with 26 surrounding quadrature points about each centroid [21]. The flux balance equation (2.5) is still valid and the time differencing is to be carried out using quadrature points on two-dimensional planes at the future time t_{n+1} and the departure times t_n−1 and t_n. Corner points of the cube may be to reduce the sizes of the coefficient matrices. However, for numerical modeling situations where high accuracies of certain feature are of paramount importance, corner points are needed to sufficiently represent the spatial dimension [20].

This method offers an effective way for sub-grid representations of local source terms to be accurately linked to the numerical solutions at grid points for multi-physics modeling problems.

6.1. Conclusion

We have demonstrated the effectiveness of the space-time unified discretization method for constructing efficient higher-order accurate implicit and explicit schemes for parabolic equations. In particular, we have described the framework for obtaining higher accuracies about the centroid of space-time control volumes that allow for effective ways to model local space-time fluxes and include sub-grid sources to improve accuracy and convergence. Using a general weighted quadrature to approximate the integral formulation allows for flexible adaptive treatments, rigorous local error analysis about each grid point, optimal choices of time step-sizes, and effective source term collocations to control the growth of the residual error terms associated with the resulting schemes. By using unified space-time expansions to approximate the solution and the local source term, robust higher-order accuracies are ensured by correctly linking the time frames and sub-grid sources effectively through the minimization of the local error.

REFERENCES

[1] A. Adcroft, C. Hill, and J. Marshall. Representation of Topography by Shaved Cells in a Height Coordinate Ocean Model. *Monthly Weather Rev.*, 125:2293–2315, 1997.

[2] C. W. Hirt A. A. Amsden and J. L. Cook. An Arbitrary Lagrangian-Eulerian Computing Method for All Flow Speeds. *J. Comput. Phys.*, 14:227–253, 1974.

[3] A. Berman and R. J. Plemmons. *Nonegative Matrices in the Mathematical sciences*. Computer Science and Applied Mathematics; A series of Monographs and textbooks. Academic Press, Inc, New York San Francisco London, 1979.

[4] C. L. Bottasso. On the computation of the boundary integral of space-time deforming finite elements. *Comm. Numer. Meth. Engrg.*, 13:53–59, 1997.

[5] D. Britz, O. Østerby, and J. Strutwolf. Damping of crank-nicolson error oscillations. *Computational biology and chemistry*, 27:253–63, 8 2003.

[6] Z. Cai, J. Mandel, and S. McCormick. The finite volume element method for diffusion equation on general triangulations. *Siam J. Numer. Anal.*, 28:392–402, 1991.

[7] M. O. Devile, P. F. Fischer, and E. H. Mund. *Higher-Order Methods for Incompressible Fluid Flow*. Cambridge University Press, Cambridge · New York · Port Melbourne · Madrid · Cape Town, 2002.

[8] C. A. J. Fletcher. *Computational Galerkin Methods*. Springer Series in Computational Physics. Springer-Verlag, New York Berlin Heidelberg Tokyo, 1984.

[9] D. A. French. A space-time finite element method for the wave equation. *Comput. Methods. Appl. Mech. Engrg.*, 107:145–157, 1993.

[10] P. Frolkovic. Maximum Principle and Local Mass Balance for Numerical Solutions of Transport Equation Coupled with Variable Density Flow. *Acta Math. Univ. Comenianae*, 1:137–157, 1998.

[11] S. Gabersek and D. R. Durran. Gap Flows through Idealized Topography. Part II: Effects of Rotation and Surface Friction. *J. Atmos. Sci.*, 63:2720–2315, 2006.

[12] Lixin Ge and Jun Zhang. Symbolic computation of high order compact difference schemes for three dimensional linear elliptic partial differential equations with variable coeffcients. *J. comput. Appl. Math*, 143:9–27, 2002.

[13] L. Gorelick, M. Blank, E. Shechtman, M. Irani, and R. Basri. Actions as Space-Time Shapes. *IEEE Trans. Pattern Analysis And Machine Intelligence*, 29:1–7, 2007.

[14] M. N. Guddati and B. Yue. Modified integration rules for reducing dispersion error in finite element methods. *Comput. Methods Appl. Mech. Engrg. 193 (2004)*, 193:275–287, 2004.

[15] T.J.R. Hughes and G.M. Huibert. Space-time finite element methods for elastodynamics: Formulations and error estimates. *Comput. Methods. Appl. Mech. Engrg.*, 66:145–157, 1988.

[16] T.J.R. Hughes and J. Stewart. A space time formulation for multiscale phenomena. *J. Comput. Appl. Math.*, 74:217–229, 1996.

[17] K. Ito, Y. Kyei, and Z. Li. Higher-Order, Cartesian Grid Based Finite Difference Schemes for Elliptic Equations on Irregular Domains . *SIAM J. Sci. Comput.*, 27:346–367, 2005.

[18] C. Kim and A. Jameson. A Robust and Accurate LED-BGK Solver on Unstructured Adaptive Meshes. *J. Comput. Phys.*, 143:598–627, 1998.

[19] Y. Kyei. Space-time finite volume differencing framework for effective higher-order accurate discretizations of parabolic equations. *SIAM J. Sci. Comput.*, 34(3):A1432–A1459, 2012.

[20] Y. Kyei. Higher-order accurate finite volume discretization of the three-dimensional poisson equation based on an equation error method. *Int. J. for Innovation Education and Research*, 6(6):107 – 123, 2018.

[21] Y. Kyei, J. P. Roop, and G. Tang. A family of sixth-order compact finite difference schemes for poisson equation. *Adv. Numer. Anal.*, Article ID 352174:1–17, 2010.

[22] M. N. Levya, R. D. Nairb, and H. M. Tufo. High-order Galerkin methods for scalable global atmospheric models. *Computers & Geosciences*, 233:1022–1035, 2007.

[23] F. Lorcher, G. Gassner, and C. D. Munz. An explicit discontinuous Galerkin scheme with local time-stepping for general unsteady diffusion equations. *J. Comput. Phys.*, 227:5649–5670, 2008.

[24] W. H. Mason. *Applied Computational Aerodynamics*. Text/notes, http://www.dept.aoe.vt.edu/ maxon/Mason f/CAtextTop.html, 1997.

[25] A. Masud and T.J.R. Hughes. A Space-time Galerkin/least-squares finite element formulation of the Navier-Staokes equations for moving domain problems. *Comput. Methods Appl. Mech Engr*, 146:91–126, 1997.

[26] C. Mattiussi. The finite volume, finite element, and finite difference methods as numerical methods for physical field problems. *Advances in Imaging and Electron Physics*, 113:1– 146, 2000.

[27] S. Mittal and T.E. Tezduyar. Notes on the stabilized space-time finite-element formulation of unsteady incompressible flows. *Comput. Phys. Commun.*, 73:93–112, 1992.

[28] E. Onate and M. Manzan. A general procedure for deriving stabilized space-time finite element methods for advective-diffusive problems. *Int. J. Numer. Meth. Fluids*, 31:203–221, 1999.

[29] W. M. Rohsenow, J. R. Hartnett, and Y. I. Cho. *Handbook of Heat Transfer*. McGraw-Hill, New York, third edition, 1998.

[30] J. Santos and P. de Oliveira. A converging finite volume scheme for hyperbolic conservation laws with source terms. *J. Comput. App. Math.*, 111:239–251, 1999.

[31] M. A. Tolstykh. Vorticity-Divergence Semi-Lagrangian Shallow-Water Model of the Sphere Based on Compact Finite Differences. *J. Comput. Phys.*, 179:180–200, 2002.

[32] E F. Toro and A. Hidalgo. ADER finite volume schemes for nonlinear reaction-diffusion equations. *App. Numer. Math.*, 59:73–100, 2009.

[33] H. van der Ven and J. J. W. van der Vegt. Space-time discontinuous Galerkin finite element method wih dynamic grid motiton for inviscid compressible flows II. Efficient flux quadrature. *Comput. Methods Appl. Mech. Engr.*, 191:4747–4780, 2002.

[34] A. K. Verma, S. M. Bhallamudi, and V. Eswaran. Overlapping control volume method for solute transport. *J. Hydr. Engrg.*, 5:308–316, 2000.